Developmental Biology 446 (2019) 119–131

Contents lists available at ScienceDirect

Developmental Biology

journal homepage: www.elsevier.com/locate/developmentalbiology

Ankyrin-G regulated epithelial phenotype is required for mouse lens morphogenesis and growth

Pratheepa Kumari Rasiah[a], Rupalatha Maddala[a], Vann Bennett[b,c], Ponugoti Vasantha Rao[a,d,*]

[a] Department of Ophthalmology, Duke University School of Medicine, Durham, NC 27710, USA
[b] Department of Biochemistry, Duke University School of Medicine, Durham, NC 27710, USA
[c] Howard Hughes Medical Institute, Duke University School of Medicine, Durham, NC 27710, USA
[d] Department of Pharmacology and Cancer Biology, Duke University School of Medicine, Durham, NC 27710, USA

ARTICLE INFO

Keywords:
Ankyrin-G
Epithelium
Cell-cell junctions
Cytoskeleton
Lens
Morphogenesis

ABSTRACT

Epithelial cell polarity, adhesion, proliferation, differentiation and survival are essential for morphogenesis of various organs and tissues including the ocular lens. The molecular mechanisms regulating the lens epithelial phenotype however, are not well understood. Here we investigated the role of scaffolding protein ankyrin-G (AnkG) in mouse lens development by conditional suppression of AnkG expression using the Cre-LoxP recombination approach. AnkG, which serves to link integral membrane proteins to the spectrin/actin cytoskeleton, was found to distribute predominantly to the lateral membranes of lens epithelium with several isoforms of the protein being detected in the mouse lens. Conditional deficiency of AnkG impaired mouse lens morphogenesis starting from embryonic stage E15.5, with neonatal (P1) AnkG cKO lenses exhibiting overt abnormalities in shape, size, epithelial cell height, sheet length and lateral membrane assembly together with defective fiber cell orientation relative to lenses from littermate AnkG floxed or Cre expressing mice. Severe disruptions in E-cadherin/β-catenin-based adherens junctions, and the membrane organization of spectrin-actin cytoskeleton, ZO-1, connexin-50 and Na^+-K^+-ATPase were noted in AnkG deficient lenses, along with detection in lens epithelium of α-smooth muscle actin, a marker of epithelial to mesenchymal transition. Moreover, lens epithelial cell proliferation and survival were severely compromised while differentiation appears to be normal in AnkG deficient mouse lenses. Collectively, these results indicate that AnkG regulates establishment of the epithelial phenotype via lateral membrane assembly, stabilization of E-cadherin-based cell-cell junctions, polarity and membrane organization of transport and adhesion proteins and the spectrin-actin skeleton, and provide evidence for an obligatory role for AnkG in lens morphogenesis and growth.

1. Introduction

Epithelial cell polarity, adhesion, proliferation, differentiation and survival are essential for morphogenesis and development of various organs and tissues including the ocular lens (Chauhan et al., 2015; Cvekl and Zhang, 2017; Pispa and Thesleff, 2003). Epithelial cell phenotype in turn is orchestrated by complex molecular and cellular machinery including different types of cell-cell junctions, lateral membrane assembly, apical and basolateral polarization, cytoskeletal organization, protein trafficking and integral membrane protein organization (Braga, 2000; Jenkins et al., 2015; Knust, 2000; Nelson et al., 2013; Pontoriero et al., 2009; Rodriguez-Boulan and Nelson, 1989). Although epithelial cell lateral membrane biogenesis and assembly, and E-cadherin-based cell-cell junctions have been demonstrated to be regulated partly by ankyrin-G (AnkG) in cell culture models, little is known about the definitive role of AnkG in epithelial organogenesis and growth (Bennett and Healy, 2009; Bennett and Lorenzo, 2016; He et al., 2014; Kizhatil et al., 2007a, 2007b). The ankyrins are a family of metazoan adaptor proteins that play a key role in linking membrane-spanning proteins, including ion channels, transporters, receptors and cell adhesive molecules to the underlying spectrin-actin cytoskeleton as well as in their micron-scale membrane organization (Bennett and Lorenzo, 2016). The ankyrin family of proteins consists of three well-characterized subtypes, including ankyrin-R (AnkR), ankyrin-B (AnkB) and AnkG, encoded by three different genes, *ANK1, ANK2, and ANK3*, respectively (Bennett and Baines, 2001; Cunha and Mohler, 2009). All three ankyrins consist of four well-conserved functional domains, including the N-terminal membrane-binding domain, spectrin binding domain, death domain and C-terminal regulatory domain (Bennett and Lorenzo, 2016). Ocular lens has been shown to express AnkB, and

* Correspondence to: Duke Eye Center, Durham, NC 27710, USA.
E-mail address: p.rao@duke.edu (P.V. Rao).

http://dx.doi.org/10.1016/j.ydbio.2018.12.016
Received 16 July 2018; Received in revised form 13 December 2018; Accepted 14 December 2018
Available online 15 December 2018
0012-1606/

AnkB deficiency has been reported to affect fiber cell cytoarchitecture, mechanical properties and membrane skeleton organization confirming its requirement for lens architecture and function (Maddala et al., 2016; More et al., 2001), however, the role of AnkG in lens development and function is not known.

Morphogenetically, the ocular lens, an avascular organ is developed from the surface ectoderm. As development progresses, lens placode which is formed from the surface ectoderm consisting of columnar cells- thickens, deepens and invaginates into lens vesicle (Cvekl and Zhang, 2017; Lovicu et al., 2011). Following the formation of lens vesicle, the posterior lens vesicle cells start to elongate and differentiate into long primary fibers extending and reaching the anterior lens vesicle cells, while the anterior lens vesicle cells form the epithelium (Chauhan et al., 2015; Cvekl and Ashery-Padan, 2014; Cvekl and Zhang, 2017; Lovicu et al., 2011). Polarity of both epithelial and fiber cells is crucial for lens development and growth (Chauhan et al., 2015; Cvekl and Zhang, 2017; Sugiyama et al., 2011; Zhang et al., 2016). Lens grows rapidly during the late embryonic and neonatal stages by epithelial cell division and differentiation. In postnatal lenses, the cell division is restricted to the germinative zone of the epithelium at the equator and as these cells divide, they differentiate into the secondary fibers (Cvekl and Ashery-Padan, 2014; Lovicu et al., 2011). The mature lens is covered with a monolayer of epithelial cells at the anterior and the rest of the lens is filled with fiber cells with different stages of differentiation and maturation. The secondary fibers as they elongate and differentiate, develop elaborate lateral membrane ball and socket interdigitations, lose all the cellular organelles and attain highly symmetric cytoarchitecture and hexagonal shape (Bassnett et al., 2011; Cvekl and Ashery-Padan, 2014). Unlike many other organs, lens grows throughout our life although at a slow rate in adult lenses compared to the young lenses (Lovicu et al., 2011). The mature lens is enclosed by a thick capsule consisting of an extracellular matrix made up of largely collagen. The basal surface of lens cuboidal epithelial cells forms adhesions with extracellular matrix of capsule, while the apical surface forms junctions with fiber cells (Sugiyama et al., 2008). The lateral membranes of lens epithelial cells develop extensive cell-cell junctions consisting of both E-cadherin and N-cadherin and their interacting partners including catenins, actomyosin and spectrin (Cheng et al., 2017; Logan et al., 2017; Rao and Maddala, 2006). These epithelial cells also develop tight junctions and gap junctions (Cvekl and Ashery-Padan, 2014; Sugiyama et al., 2008; White et al., 2007).

In this study, we used the ocular lens as a model system to investigate the role of AnkG in epithelial organogenesis and tissue architecture, since this organ maintains a highly polarized epithelium (Cvekl and Zhang, 2017; Pontoriero et al., 2009). Our approach to inducing conditional deficiency of AnkG in the developing lens not only revealed a crucial role for AnkG in lens morphogenesis but also a requirement for this protein in the organization of epithelial cell lateral membrane complexes and cell-cell junctions, and epithelial cell polarity, proliferation and survival, providing in vivo evidence for an essential role for AnkG in epithelial phenotype establishment and lens morphogenesis and growth.

2. Materials and methods

2.1. Mice

Mice were maintained in a pathogen-free vivarium under a 12 h dark and light cycle with ad libitum food and water as we described earlier (Maddala et al., 2015). All experiments using mice were carried out in accordance with the recommendations of the Guide for the Care and Use of Laboratory Animals of the National Institutes of Health and the Association for Research in Vision and Ophthalmology. The protocol was approved by the Institutional Animal Care and Use Committee (IACUC) of the Duke University School of Medicine.

2.2. Generation of ankyrin-G conditional knockout (AnkG cKO) mice

AnkG cKO mice were developed by mating AnkG floxed mice (with loxP sites flanking exon 22 and 23 of the *ANK3* gene; maintained on a C57BL/6J background) obtained from Vann Bennett (Jenkins et al., 2013), Duke University, with lens-specific Cre recombinase expressing transgenic mice (Le-Cre mice) as described earlier (Maddala et al., 2015). The Le-Cre transgenic mice used in this study express Cre recombinase at embryonic day 8.75 under the control of a Pax6 P0 enhancer/promoter, with Cre being expressed in lens epithelium and fiber cells as well as other surface ectoderm-derived eye structures (Ashery-Padan et al., 2000). For comparison with AnkG cKO mice (F4 and above generation), we used littermate AnkG floxed controls that were negative for the Cre transgene. Tail DNA derived from progeny was screened for the AnkG floxed alleles and Cre transgene by PCR analysis as described earlier by us (Maddala et al., 2015).

2.3. RT-PCR and qRT-PCR

To determine the relative expression level of different AnkG gene splice variants in mouse lens, total RNA was extracted from neonatal (P1) mouse lenses (pooled) using an RNeasy Micro kit (Cat. No. 74004; Qiagen, Inc., Valencia, CA, USA) and reverse transcribed using the Advantage RT for PCR Kit (Cat. No. 639506; Clontech Laboratories, Inc., Mountain View, CA, USA), as we described previously (Maddala et al., 2015). Reverse-transcribed single-stranded cDNA, different region-specific forward and reverse oligonucleotide PCR primers of AnkG (Supplementary Table 1S) and PrimeSTAR GXL DNA Polymerase PCR kit (Cat no. R050A; Clontech Takara; Mountain View, CA, USA) were used to amplify different splice variants of AnkG. Amplified DNA products were separated by agarose gel electrophoresis and visualized using Gel Red Nucleic Acid Stain (Cat. No. 41002; Biotium, Hayward, CA, USA) and Viewed with Bio-Rad ChemiDoc™ Touch Imaging System; Hercules, CA. The DNA products were sequenced to confirm their identity.

For qRT-PCR analysis of the relative expression of AnkG and AnkB in the mouse lens of P2 and P30, the qRT-PCR reactions were set up using a CFX 96™ Real-Time PCR detection system (Bio-Rad Hercules, CA, USA) and the respective specific oligonucleotide primer sets (Supplementary Table 1S). Fold differences in AnkG and AnkB gene expression in P2 and P30 mouse lenses were normalized to glyceraldehyde 3-phosphate dehydrogenase (GAPDH) and calculated by the comparative threshold (CT) method, as described by the manufacturer.

2.4. Histological analysis

Embryonic heads (E15.5) and whole eyes (from postnatal P1, P10 and P21 mice) were fixed for 48 h at room temperature in 3.7% buffered formalin as we described earlier (Maddala et al., 2015). AnkG cKO and respective littermate control specimens were subsequently dehydrated, embedded in paraffin, and cut in 5 μm thick sections with a rotary microtome (Leica Biosystems, Buffalo Grove, IL, USA), prior to staining with hematoxylin and eosin as described earlier (Maddala et al., 2011). Images were captured using Zeiss Axio Imager equipped with a Hamamatsu Orca ER monochrome CCD camera.

2.5. Tissue fixation and immunofluorescence

Embryonic, neonatal and post-natal mouse eyes were fixed for cryostat or paraffin sectioning. For tissue frozen sectioning, embryonic heads and eyes were fixed in 4% buffered paraformaldehyde for 24 h at 4 °C, transferred into 5% and 30% sucrose in PBS (phosphate buffered saline) on successive days, embedded in optimal cutting temperature (OCT) embedding media (Tissue-Tek, Torrance, CA, USA), and cut into 8- to 10-μm-thick sections using a Microm™ HM550 Cryostat (GMI, Ramsey, MN, USA), as we previously described (Maddala et al., 2015).

For paraffin sections, tissue specimens were fixed in 3.7% buffered formalin, embedded in paraffin, and cut into 5-μm-thick sections as we described previously (Maddala et al., 2011).

Air-dried tissue cryosections (sagittal plane) were treated with Image-iT FX signal enhancer (Invitrogen, Eugene, OR, USA) and blocked using blocking buffer (5% globulin-free BSA and 5% filtered goat serum in 0.3% Triton X-100 containing PBS) for 30 min each as we described earlier (Maddala et al., 2011). Tissue sections were then incubated overnight at 4 °C with appropriate dilutions of primary antibodies in blocking buffer, including AnkG, E-cadherin, αE-catenin, AnkB, ZO-1, connexin-50, Na/K-ATPase, β-catenin, aquaporin-0, laminin, γ-crystallin and Ki67 (see Supplementary Table 2S for the details). Sections were then washed in 0.3% Triton X-100 containing PBS prior to incubation with appropriate Alexa Fluor (488 or 594)–conjugated secondary antibodies (Invitrogen, Grand Island, NY, USA; at a 1: 200 dilution). For α-smooth muscle actin and F-actin staining, preblocked sections (cryo) were labeled with Cy3-conjugated α-SMA antibody (1: 200 dilution, Table 2S) and tetramethyl rhodamine isothiocyanate–conjugated phalloidin (TRITC; 1:500 dilution), respectively, for 2 h at room temperature, washed, and mounted as described above. Tissue sections were also stained with wheat germ agglutinin-TRITC and CellBrite red stain (Table 2S). All representative immunofluorescence and fluorescence data reported in this study are based on analysis of a minimum of three tissue sections derived from three independent specimens. Images were captured using an Eclipse 90i confocal laser scanning microscope (Nikon Instruments, Inc., Melville, NY, USA).

For paraffin sections, deparaffinization and antigen retrieval were performed as we described earlier (Maddala et al., 2016). Tissue sections were blocked for 10 min in a humidified chamber with background Sniper solution (Biocare Medical, Concord, CA, USA), prior to incubation for 24 h at 4 °C with appropriate primary antibodies (N-cadherin, ezrin, β-spectrin, AnkG, β-actin, β-catenin, Zo-1, Na/K-ATPase and E-cadherin; details are described in Supplementary Table 2S). Tissue sections were washed in TBS (Tris-buffered saline) buffer and incubated with either Alexa Fluor 488– or 594–conjugated secondary antibodies in a dark humidified chamber for 2 h at room temperature. After this, sections were washed again with TBS buffer, and slides were mounted using Vecta mount and nail polish prior to being imaged using a Nikon Eclipse 90i confocal laser scanning microscope, to obtain single optical images and Z-stacks as previously described by us (Maddala et al., 2016). Fluorescence quantification was performed using NIS-Elements imaging software version 4.5 (Nikon Instruments Inc. Melville, NY. USA).

2.6. Immunoblotting

To determine the different protein products of splice variants of AnkG gene in P1 and P21 mouse lenses, lens lysates (800 × *g* supernatant) were prepared in protein solubilization buffer containing 8 M Urea, 5% SDS, 50 mM Tris pH7.4, 5 mM EDTA, 2.5 mM N-ethylmaleimide, along with complete Mini, EDTA-free protease Inhibitor cocktail tablet and PhosSTOP phosphatase inhibitor cocktail tablet, 1 per 10 ml buffer, respectively (Roche, Manheim, Germany). Protein quantification was performed using Micro BCA™ protein Assay Kit (Cat. no. 23235; Thermo Fisher Scientific, Waltham, MA. USA), equal amount of protein (20 μg) was mixed thoroughly with freshly prepared 5× SDS/PAGE Laemmli buffer with 40 mM DTT (dithiothreitol) and incubated for 10 min at 65 °C, and followed by separation on 4–20% Mini-Protean® TGX Stain-Free™ gradient SDS-polyacrylamide gel (Bio-Rad Hercules, CA, USA) and electrophoretically transferred to nitrocellulose membrane (Bio-Rad). Nitrocellulose membranes were probed with polyclonal AnkG antibody provided by Vann Bennett from Duke University (Supplementary Table 2S) and subsequently with appropriate secondary antibody as we described earlier (Maddala et al., 2016). Blots were developed by chemiluminescence using Chemidoc™ Touch (Bio-Rad), and bands were quantified using ImageJ Software. GAPDH was immunoblotted as a loading control using anti-GAPDH antibody (Table S2), where required.

2.7. TUNEL assay

To evaluate and compare apoptotic cell death in AnkG cKO and littermate control mouse lenses, tissue cryosections were subjected to in-situ Terminal deoxynucleotidyl Transferase dUTP Nick End Labeling (TUNEL) using an ApopTag Plus Fluorescein Kit (EMD Millipore, Burlington, MA, USA) as we described earlier (Maddala et al., 2015). TUNEL labeled tissue sections were counter-stained with propidium iodide. Imaging was performed using a Nikon Eclipse 90i confocal microscope and counted manually.

2.8. Statistical analysis

All data are reported as the mean ± SEM values calculated from at least 5 independent samples. Comparisons between two groups were performed using the Student's *t*-test, with values of *P < 0.05 being considered statistically significant.

A Key Resources Table (KRT) for easy discovery is included.

Key Resource Table

Reagent or Resource	Source	Identifier
Antibodies		
Ankyrin-G (rabbit Polyclonal)	The Vann Bennett laboratory Duke University, Durham, NC	
β-Actin (mouse monoclonal)	Cell Signaling Technologies, Inc. Danvers, MA.	8H10D10
β2-Spectrin (mouse monoclonal)	BD Biosciences, San Jose, CA.	612563
Ezrin (mouse monoclonal)	Sigma/Aldrich, St. Louis, MO	E8897
E-Cadherin (rabbit Polyclonal)	Cell Signaling Technology, Inc. Danvers, MA.	3195S
E-Cadherin (mouse Polyclonal)	Life Technologies Corporation, Grand Island, NY	MA5-12547
N-cadherin (mouse monoclonal)	Life Technologies Corporation, Grand Island, NY	33–3900
β-catenin (rabbit Polyclonal)	Cell Signaling Technologies, Inc., Danvers, MA	9562
β-catenin (mouse monoclonal)	Sigma/Aldrich, St. Louis, MO	C7207
αE-catenin (rabbit Polyclonal)	Cell Signaling Technologies, Inc., Danvers, MA	3236
ZO-1 (rabbit Polyclonal)	Cell Signaling Technologies, Inc., Danvers, MA	13663
ZO-1 (Rat monoclonal)	Developmental Studies Hybridoma Bank., Iowa City, Iowa.	R26.4C
Connexin-50 (rabbit Polyclonal)	Alpha Diagnostic Intl. Inc., San Antonio, Texas	Cx50-A
Na^+-K^+-ATPase (mouse monoclonal)	Novus Biologicals, LLC, Littleton CO	NB300-

		146SS
α-smooth muscle actin- Cy3 conjugated	Sigma/Aldrich, St. Louis, MO	C6198
Ankyrin-B (rabbit Polyclonal)	The Vann Bennett laboratory Duke University, Durham, NC	
Ki67 (rabbit Polyclonal)	Cell Signaling Technologies, Inc, Danvers, MA	9129
γ-Crystallin	The Sam Zigler Laboratory, Johns Hopkins University School of Medicine. Baltimore, MD	
Aquaporin-0	The Joe Horwitz laboratory, Jules Stain Eye Institute, UCLA. CA	
Phalloidin–Tetramethylrhodamine B isothiocyanate (TRITC)	Sigma/Aldrich, St. Louis, MO	P1951
CellBriteTM Orange cytoplasmic membrane dye	Biotium, Inc., Fremont, CA	30022
Lectin TRITC labeled from Triticum vulgaris	Sigma/Aldrich, St. Louis, MO	L5266
Laminin	The Harold Erickson laboratory, Duke University, Durham, NC	
GAPDH (mouse monoclonal)	Proteintech Group, Chicago, IL	60004-1
qRT-PCR Oligonucleotides		
AnkG 5′-ACCAGGCTCGGGATTCTATTA-3′ 5′-GGGTTTAGGTGCGTCTTCTAT-3′	Integrated DNA Technologies, Inc. Skokie, IL	
5′-CCTGAAGGTTGTGACTGAAGAG-3′ 5′-CACGGGCATCCACCATAAA-3′	Integrated DNA Technologies, Inc. Skokie, IL	
RT-PCR Oligonucleotides		
AnkG PS1 5′-GCGGAAGAAGAGACTGAGAAA-3′ 5′-TCCTGCTTAATCCGGGAAAC-3′	Integrated DNA Technologies, Inc. Skokie, IL	
AnkG PS2 5′-TAGCCAGTAGGCTGGTAGAA-3′ 5′-TCGTGAAATAACGGCTTAGGG-3′	Integrated DNA Technologies, Inc. Skokie, IL	
AnkG PS3 5′-GATGGAGAGGAGAGACAGAAGA-3′ 5′-AAGTGCTGGCTCTCAACTAC-3′	Integrated DNA Technologies, Inc. Skokie, IL	
AnkG PS4 5′-GAACGGCTCTCTCTCAGAAATTA-3′ 5′-CTTCTCCACGTTCCGGATTT-3′	Integrated DNA Technologies, Inc. Skokie, IL	
Critical Commercial Assay used		
ApopTag® Plus In Situ Apoptosis Fluorescein Detection Kit	MilliporeSigma, Burlington Massachusetts	S7111
Experimental Models: Organisms/Strains		
AnkG Floxed mice	The Vann Bennett laboratory Duke University, Durham, NC	
Le-Cre transgenic mice	The Michael L. Robinson laboratory, Miami university, Miami, originally developed by, Ruth Ashery-Padan, Ph.D	
Reagents:		
Background Sniper	Biocare Medical, Concord, CA.	BS966L
PageRuler™ unstained Protein Ladder, 10–250 kDa	ThermoFisher Scientific, Waltham, MA.	26614

3. Results

3.1. AnkG exhibits preferential distribution to the epithelium in mouse lens

The ocular lens is a transparent and epithelial cell-derived simple organ that has been extensively exploited as a model system to identify the various molecular mechanisms involved in organ morphogenesis, differentiation, growth and architecture (Chauhan et al., 2015; Cvekl and Ashery-Padan, 2014; Cvekl and Zhang, 2017). While AnkB has been demonstrated to play a crucial role in lens fiber cell cytoarchitecture and membrane organization (Maddala et al., 2016; More et al., 2001), nothing is known about the possible involvement of AnkG in lens development, growth or function. As a matter of fact, one previous study has reported that AnkG is not detectable in the lens tissue (More et al., 2001). Contrary to this prior observation, our recent mouse lens cDNA microarray analysis detected AnkG expression in mouse lens, although the levels of AnkG were nearly 6-fold lower than those of AnkB expression (Maddala and Rao, 2017) based on relative signal intensity values. Since our previous study reported that AnkB plays a crucial role in lens architecture via primarily regulating fiber cell cytoarchitecture, with not much influence either on lens epithelium or morphogenesis (Maddala et al., 2016), we asked what, if any role AnkG played in the lens and whether the role of AnkG could be distinct from the known role of AnkB. To investigate these unexplored aspects, and to confirm cDNA microarray data from our previous study (Maddala and Rao, 2017), we initially performed qRT-PCR analysis of AnkG and AnkB expression in both neonatal (P2) and one month-old (P30) mouse lenses. In these analyses we found that while the expression levels of AnkG and AnkB are very similar in neonatal (P2) lenses, AnkG expression was dramatically reduced (by ~ 80%) in P30 lenses relative to the level of AnkB, indicating a developmental and maturation-dependent downregulation of AnkG expression in the mouse lens (Fig. 1A, values are based on duplicate analyses from two independent samples). We then performed immunoblotting analysis of AnkG protein isoforms in both P1 and P21 mouse lens homogenates, using an AnkG polyclonal antibody and comparing results to those derived from brain tissue homogenate samples (2 μg protein) of the same animals. Consistent with the qRT-PCR results, AnkG protein levels were also found to be dramatically reduced (by ~ 85%) in P21 lenses compared to P1 lenses (Fig. 1B and C). Several prominent AnkG immunopositive bands were detected in P1 mouse lens homogenates (two pooled samples analyzed), with molecular mass ranging from 50 kDa to > 200 kDa. These included relatively intense bands at ~ 200 kDa (doublets), 105 kDa and weak bands at ~ 85 and 60 kDa, indicating the presence of protein products potentially corresponding to several splice variants of the AnkG gene (Fig. 1B), or of posttranslationally modified isoforms. Brain tissue samples (two individual samples) exhibited not only the same profile of AnkG protein bands as that in the lens, but contained additional and distinct bands with molecular mass greater than 300 kDa (Fig. 1B). Unlike brain tissue which exhibits one intense immunopositive AnkG band at ~ 200 kDa, lens samples consistently revealed the presence of a band at ~ 200 kDa and a second closely migrating protein with slightly higher molecular

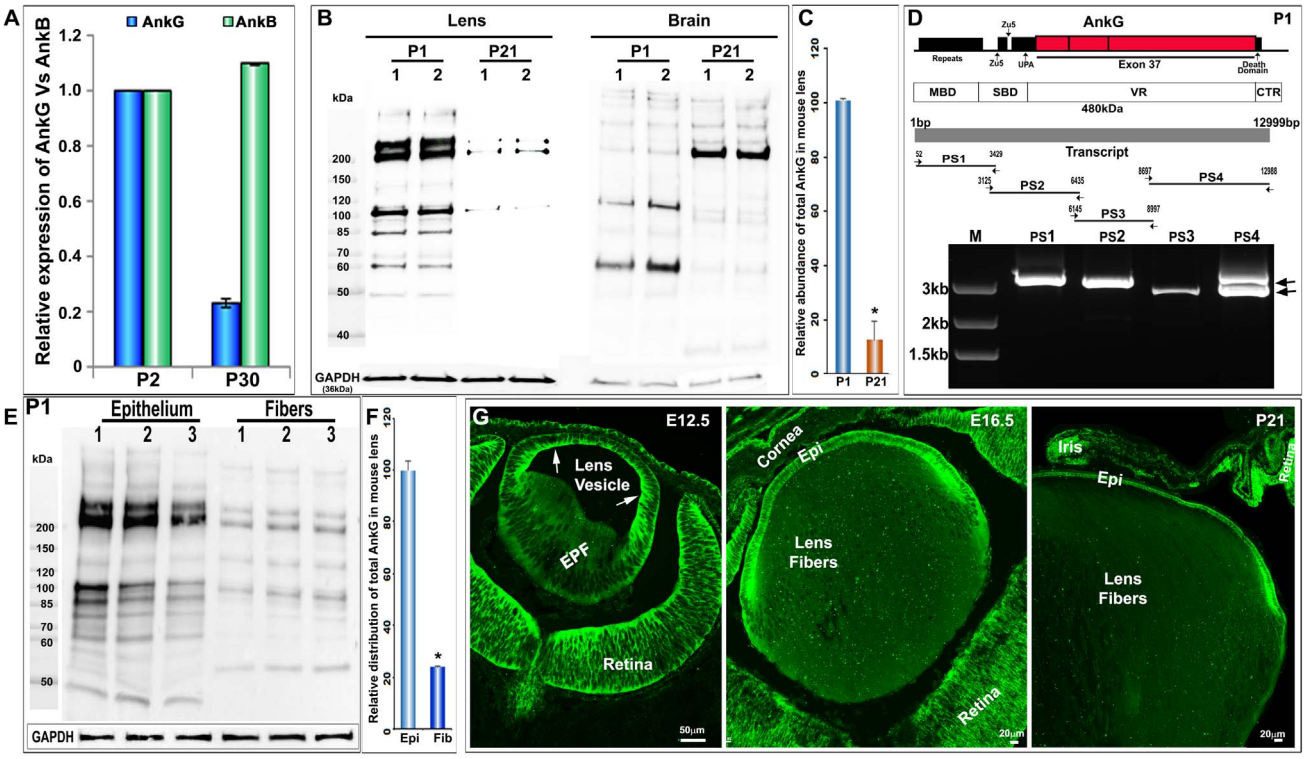
A
AnkG
AnkB
Relative expression of AnkG Vs AnkB
P2
P30
B
Lens
Brain
P1
P21
kDa
GAPDH
C
Relative abundance of total AnkG in mouse lens
D
AnkG
P1
Repeats
Exon 37
Death Domain
MBD
SBD
VR
CTR
480kDa
Transcript
PS1
PS2
PS3
PS4
M
3kb
2kb
1.5kb
E
Epithelium
Fibers
F
Relative distribution of total AnkG in mouse lens
Epi
Fib
G
E12.5
Lens Vesicle
EPF
Retina
E16.5
Cornea
Epi
Lens Fibers
Retina
P21
Iris
Epi
Retina
Lens Fibers
50μm
20μm

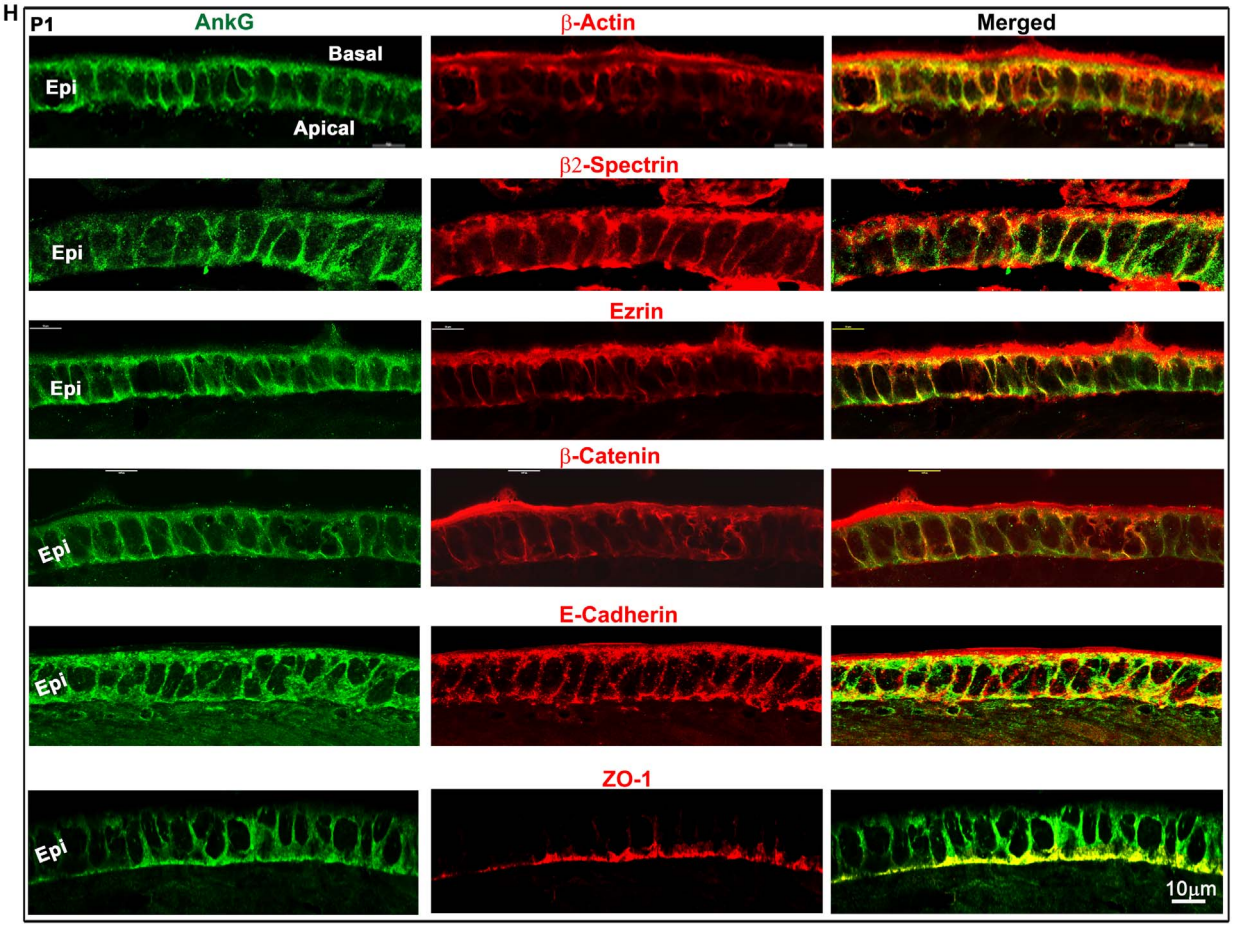
H
P1
AnkG
β-Actin
Merged
Basal
Apical
Epi
β2-Spectrin
Ezrin
β-Catenin
E-Cadherin
ZO-1
10μm

Fig. 1. Developmental regulation of expression and preferential distribution of AnkG to the epithelium, and colocalization of AnkG with cell junctional proteins and the spectrin/actin cytoskeleton in mouse lens. A). Expression and distribution of AnkG in developing and mature mouse lenses was performed by q-RT-PCR analysis relative to AnkB, using RNA derived from the P2 and P30 lenses. B). AnkG immunoblot analysis of P1 and P21 lenses derived from two independent specimens compared to brain tissue of the same animals. C). Relative levels of AnkG (total) protein in P1 and P21 lenses. D). RT-PCR analysis of various splice variants of AnkG gene expression based on walk-through amplification using distinct primer sets (PS1–4) spanning the entire coding sequence of the 480 kDa (longest) AnkG mRNA and RNA prepared from P1 mouse lenses. The top panel is a schematic of the 480 kDa form of AnkG with giant inserted exon 37 adopted from Tseng et al. (2015), and below it is a schematic of the membrane binding domain (MBD), spectrin binding domain (SBD), variable region (VR) and C-term domain (CTD) of AnkG protein. The double arrows in the bottom panel indicate two closely migrating, distinct DNA products). E & F). Immunoblotting analysis of distribution of AnkG in the mouse lens epithelium and fiber fractions derived from three independent pooled specimens of P1 lenses and its relative levels in these fractions. G). Immunofluorescence analysis of distribution of AnkG in the developing lenses from E12.5 and E16.5 embryonic and P21 mice (arrows indicate discrete distribution of AnkG to the presumptive lens epithelium), and H). Immunofluorescence analysis of the colocalization of AnkG with E-cadherin, β-catenin, Zo-1, ezrin, β-spectrin and β-actin in the lens epithelium of P1 mouse. GAPDH was immunoblotted as a loading control in data shown in panels B & E. Where indicated scale bars represent image magnification, with the molecular mass of proteins reported in kDa units and nucleotide base pairs of amplified DNA product reported as kb units. EPF: Elongating primary fibers, Epi: Epithelium.

mass than 200 kDa. We believe that the intense bands (~ 200 kDa) found in both lens and brain tissue is the well characterized brain abundant, 190 kDa form of AnkG (Kordeli et al., 1995). The second intense protein band (upper band in the 200 kDa doublet) observed in the lens sample could be a splice variant of the 190 kDa form of AnkG. Additionally, we performed RT-PCR analysis of P1 lenses to characterize expression profiles of different splice variants of the AnkG gene, using 4 different overlapping PCR primer sets covering the entire sequence of the mRNA of the longest AnkG (480 kDa) isoform (1–12,999 bp). This analysis showed a robust amplification of DNA products corresponding to primer sets 1 (from 52 to 3429 bp), 2 (from 3125 to 6435 bp) and 4 (from 8697 to 12,988 bp) relative to primer set 3 (from 6145 to 8997 bp) (Fig. 1D). Primer set 4 yielded two individual but closely migrating DNA products (indicated by arrows in Fig. 1D). These results confirm the expression of AnkG splice variants encoded by exon 37 (brain-specific) as well in neonatal mouse lens.

Having noted readily detectable levels of AnkG protein in the mouse lens, we decided to examine the tissue distribution of AnkG within the lens. To do this, we isolated the epithelium from P1 mouse lenses by separating the lens capsule (to which the epithelium is attached) from the lens fibers. When both lens epithelium (pooled from 6 lenses) and fiber mass (pooled from two lenses) lysates were probed for AnkG protein by immunoblot analysis, AnkG was detected predominantly in the epithelial fraction, with significantly lower levels (75% lower based on total AnkG immunopositive staining) found in the lens fiber mass (Fig. 1E and F). Additionally, immunofluorescence analysis of AnkG in E12.5, E16.5 and P21 mouse lens cryosections (Fig. 1G) revealed that this protein exhibits preferential distribution to the epithelium relative to lens fiber cells, corroborating the immunoblot results described above (Fig. 1E). It should be noted that in early embryonic mouse lens (E12.5), AnkG was found to be distributed relatively intensely to the apical regions of the lens epithelial cells as shown in Fig. 1G (arrows). The apical distribution pattern of AnkG was confirmed in additional specimens derived from the E11.5 and E13.5 mouse lenses by

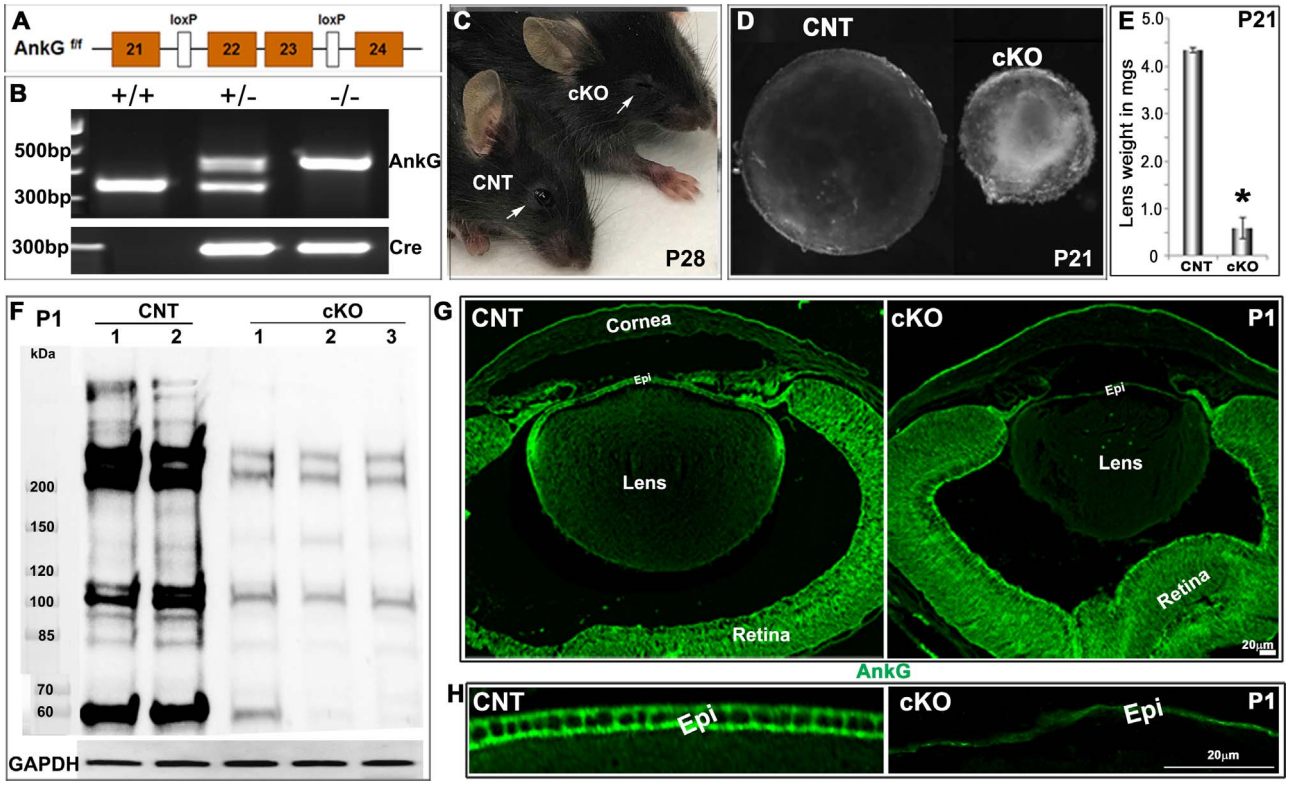

Fig. 2. LoxP-Cre recombination-mediated conditional deficiency of AnkG in the ocular lens of mice results in microphthalmia and a cataract phenotype. To determine the role of AnkG in lens development, growth and function, an AnkG conditional knockout mouse model was generated by crossing floxed AnkG mice with Le-Cre transgenic mice. A). indicates the location of loxP sites in AnkG gene. B). PCR –based genotype analysis confirming the generation of homozygous AnkG cKO mice. C & D). P28 AnkG cKO mice (> F4 generation) exhibit bilateral microphthalmia (C) and cataract (D) and significantly decreased lens weight (E; n = 6, *P < 0.05) compared to littermate AnkG floxed control (CNT) mice. F). Immunoblot analysis confirming the deficiency of AnkG (by > 80%) in P1 AnkG cKO mouse lenses (three independent samples) relative to littermate control mouse lenses (data from 2 independent specimens). GAPDH was immunoblotted as a loading control. G). Confirmation of absence of AnkG specific immunofluorescence in P1 AnkG cKO mouse lenses relative to other ocular tissues and in comparison with littermate control mouse lenses. H). Magnified images of the lens epithelium immunostained for AnkG from control and AnkG cKO mice. Scale bars in panels G & H indicate image magnification.

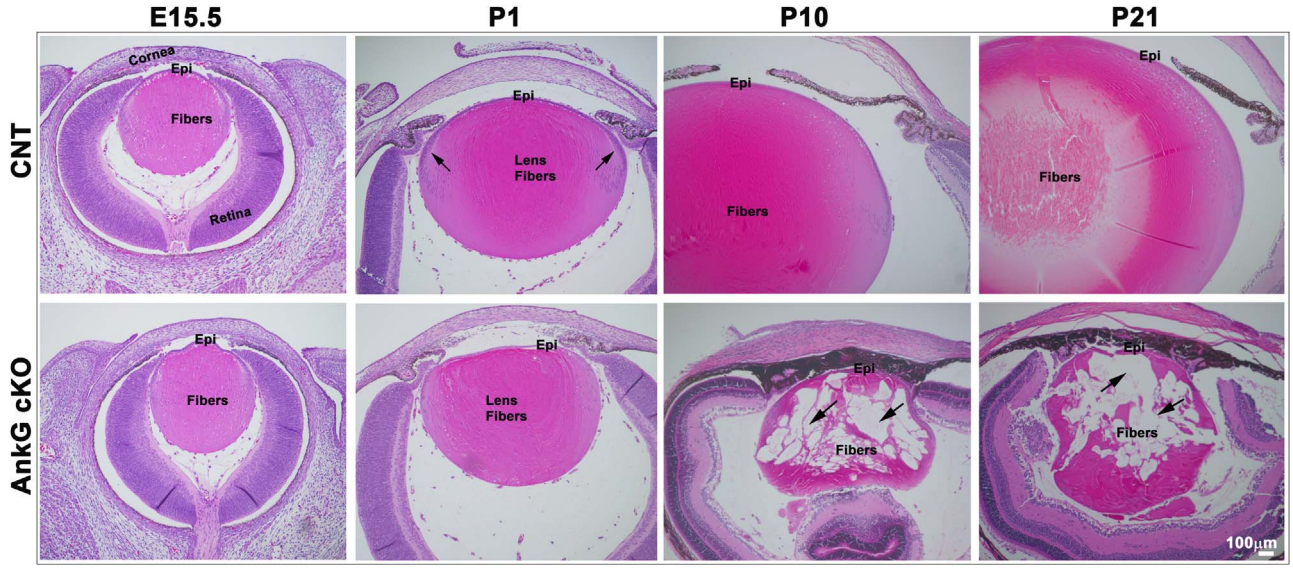

Fig. 3. AnkG cKO mouse lenses reveal progressive and extensive histological abnormalities. To determine AnkG deficiency-induced changes in lens morphogenesis and integrity, eyes derived from E15.5, P1, P10 and P21 AnkG cKO and corresponding littermate control (AnkG floxed) mice were fixed, and paraffin embedded sections (sagittal plane) were stained with hematoxylin and eosin for histological analysis. Representative images are shown to depict the progressive histological changes in lens integrity at different stages between E15.5 and P21. Starting from P1, lens fiber cell organization, lens shape, size and epithelial width and length were found to be abnormal in AnkG cKO specimens, together with accumulation of large vacuoles (indicated with arrows) and complete degeneration of the lens in P10 and P21 mice compared to those from littermate controls. Arrows in the P1 specimen indicate lens fulcrum in control mice and an abnormal fulcrum in AnkG cKO mice. Scale bar indicates image magnification.

immunofluorescence detection (Supplemental material; Fig. 1S). In contrast to AnkG, AnkB has been shown to distribute to both epithelium and fiber cells in mouse lens (Maddala et al., 2016; More et al., 2001). Within the lens epithelium of P1 specimens, AnkG appears to localize to the basal, apical and lateral membranes, colocalizing with β-actin, β-spectrin, ezrin, E-cadherin, β-catenin and Zo-1, as shown in Fig. 1H. In addition to P1 specimens, we also examined the distribution pattern of AnkG in E15.5 and P21 lens epithelium and found that AnkG distribution in E15.5 lenses is identical to that seen in P1 lenses, colocalizing with E-cadherin and β-catenin (Fig. 2S). However, unlike the columnar morphology observed for lens epithelium from E15.5 and P1 specimens, epithelial cells from P21 specimens attain a cuboidal shape with relatively reduced levels of AnkG (75% decrease based on immunofluorescence staining) and colocalizing with E-cadherin and β-catenin (Fig. 2S). In P21 mouse lens epithelium, although AnkG immunofluorescence was reduced relative to E15.5 and P1 specimens, there was detectable AnkG staining distributing to the apical regions (Fig. 2S).

3.2. Conditional deficiency of AnkG impairs lens morphogenesis, growth, shape and integrity

To investigate the functional significance of the preferential distribution of AnkG to lens epithelium, we generated mice with conditional deficiency of AnkG expression in the lens tissue by crossing AnkG floxed mice (*Ank3*$^{flox/flox}$) with loxP sites flanking exon 22 and 23 of the *Ank3* gene, and Cre recombinase transgenic mice (Le-Cre mice) expressing Cre in a lens specific manner as we described earlier (Maddala et al., 2015). Fig. 2A & B show the position of the loxP sites in the AnkG gene and confirmation of conditional deletion of AnkG based on tail DNA genotyping, respectively. The postnatal (data are shown for P28 & P21) mice with AnkG floxed allele and expressing Cre recombinase maintained on a C57BL/6J genetic background (> F4 generation) consistently exhibit bilateral microphthalmic eyes with smaller lenses and opacification (Fig. 2C–E). This phenotype was observed only in the homozygous AnkG floxed allele mice expressing Cre. Hereafter these AnkG floxed and Cre expressing mice will be referenced as AnkG cKO mice. Mouse lenses from neonatal (P1) AnkG cKO animals were confirmed to be deficient in AnkG protein by immunoblotting (85% decrease relative to controls; n = 4; Fig. 2F) and immunofluorescence (Fig. 2G) analyses. All the major AnkG protein isoforms detected in the littermate control mouse lenses were found to be dramatically reduced in the AnkG cKO mouse lenses. AnkG specific immunofluorescence was similarly confirmed to be either absent or markedly reduced in AnkG cKO lenses compared to littermate controls (AnkG floxed) or Cre transgenic mouse lenses (comparative data are shown relative to littermate control specimens). There also seems to be some reduction in AnkG expression in tissues of the iridocorneal angle including trabecular meshwork, iris and ciliary muscle in AnkG cKO mouse eyes, relative to littermate controls (Fig. 2G). The lens weight of P21 AnkG cKO mice was reduced by more than 80% compared to littermate control mouse lenses (Fig. 2E; n = 6) and Fig. 2H shows the magnified epithelium of the AnkG cKO mouse lens immunostained for AnkG relative to a littermate control specimen.

To determine the impact of AnkG deficiency on lens morphogenesis, growth and architecture, we performed a histological analysis of paraffin fixed and hematoxylin and eosin stained sagittal sections of embryonic (E15.5), neonatal (P1), weanling (P10) and P21 AnkG cKO mouse eyes, and littermate control eyes. The results revealed that AnkG cKO mouse lenses exhibit an altered shape and decreased size, together with an age-dependent progressive degeneration and accumulation of large vacuoles in fibers, starting from day E15.5 (Fig. 3). Having confirmed a lens phenotype in the AnkG cKO mice which is evident starting from the embryonic and neonatal stages, we used only eye specimens from the P1 and E15.5 embryonic stages of AnkG cKO mice for all further analyses, focusing on immunofluorescence analysis. In P10 and P21 AnkG cKO mouse eyes, it was observed that the iris was frequently fused with the lens (Fig. 3). Additionally, fulcrum formation (Sugiyama et al., 2009) was found to be either impaired or lacking in P1 AnkG cKO mouse lenses (Fig. 3, indicated with arrows, also see Supplemental material for additional images; Fig. 7S).

3.3. AnkG absence impairs lens epithelial phenotype establishment, lateral membrane assembly, cell-cell junctions and membrane organization of the actin-spectrin cytoskeleton and integral proteins

Some of the striking and consistent phenotypic deficits observed in P1 AnkG cKO mouse lenses were thinning of the epithelium and

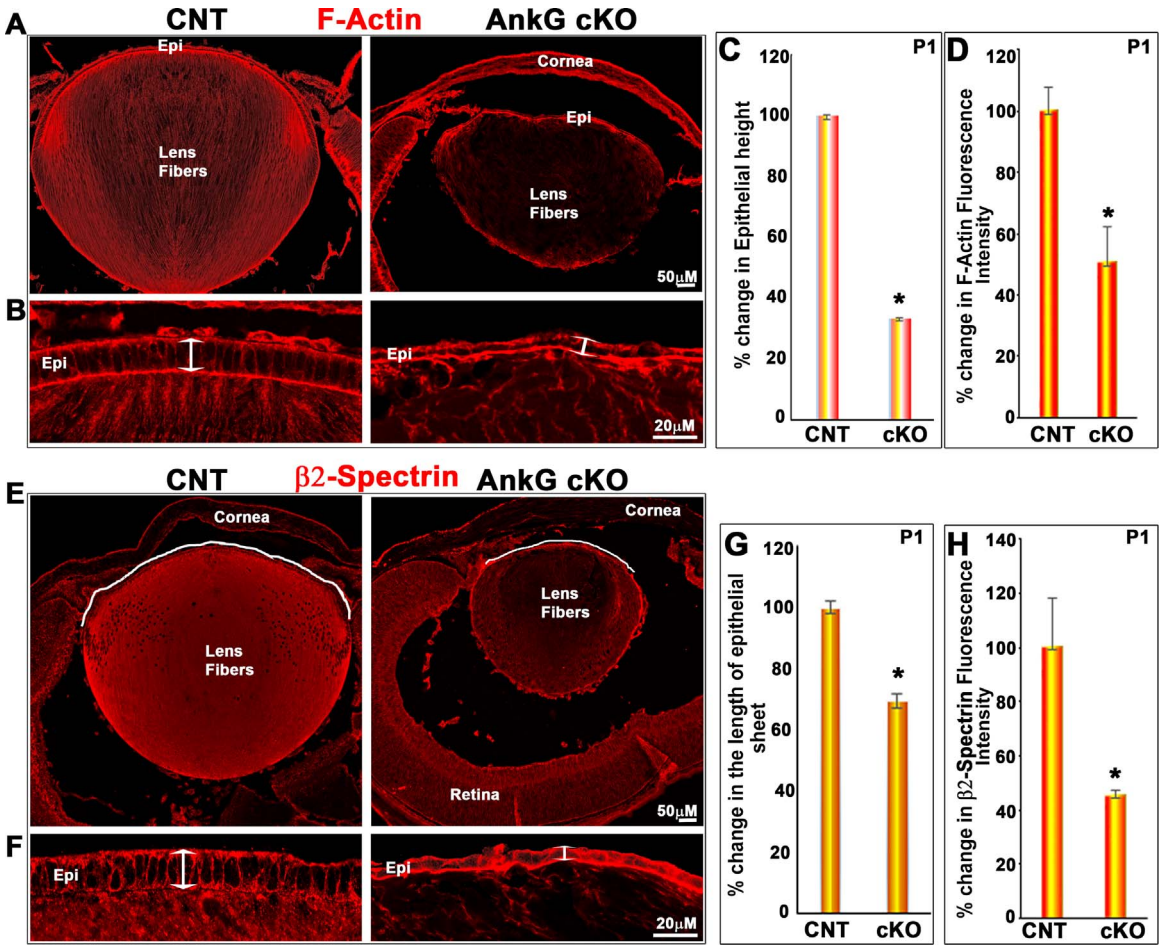

Fig. 4. AnkG deficiency impacts lens epithelial height and length, and disrupts the spectrin-actin cytoskeletal organization in mice. To quantitate the changes in lens epithelial height and sheet length induced by AnkG deficiency, P1 eyes derived from AnkG cKO and littermate control mice were fixed for cryo- and paraffin-sectioning prior to staining and image analysis. A). Sagittal sections were stained for F-actin (cryosections stained using rhodamine-phalloidin or E). immunostained for β-spectrin (paraffin sections). B). Magnified images of the lens epithelium stained for F-actin and F). β-spectrin were used to measure the height of the columnar epithelium (indicated with double head arrows). C). The height of the lens epithelium in AnkG cKO mice was significantly shorter (by ~ 70%; n = 6; *P < 0.05) compared to the corresponding control (CNT) specimens. G). Similarly, the length of lens epithelial sheet (indicated with white line) was found to be significantly shorter (by 38%, n = 6; *p < 0.5) in AnkG cKO mice compared to control specimens. Additionally, while staining of both F-actin (B) and β-spectrin (F) distributes intensely to the basolateral membrane, apical membrane and cell-cell junctions in the lens epithelium of control mouse lenses, it is markedly disrupted in AnkG cKO specimens due to the lack of lateral membrane complexes and cell-cell junctions. Moreover, the overall staining intensity for both F-actin (panel D) and β-spectrin (panel H) is also significantly reduced by ~ 50% throughout the AnkG cKO mouse lens including the fiber cells, as compared to control (CNT) mice, indicating disruption of organization of the actin and spectrin cytoskeleton under AnkG deficiency. Scale bars represent image magnification.

shortening of the epithelial sheet length (Fig. 4). The height of the columnar lens epithelium was significantly reduced (by > 60%) compared to control lenses (Fig. 4B, C and F; specimens labeled for F-actin or β2-spectrin; values based on n = 6). Similarly, epithelial sheet length in the AnkG cKO mouse lenses was also significantly reduced (by nearly 30%) compared to control specimens (Fig. 4E and G; specimens immunolabeled for β2-spectrin, the white line depicts length of the epithelial sheet; values were based on n = 6), owing to which AnkG cKO mouse lenses were frequently found to exhibit a conical shape instead of the typical spherical shape of wild type lenses. Disruptions in lens epithelial columnar shape and polarity appear to start beginning from the E15.5 stage in AnkG cKO mice compared to controls (see Supplemental figure; Figs. 4S and 8S, specimens were stained with WGA and CellBrite, respectively). Additionally, as shown in Fig. 4A, P1 AnkG cKO mouse lenses (sagittal sections) exhibited significantly decreased staining for both F-actin (Rhodamine-phalloidin staining; Fig. 4A and D) and β2-spectrin (Fig. 4E and H) relative to control specimens (by ~ 50%) indicating disruption of the actin-spectrin membrane skeleton organization under deficiency of AnkG.

Another prominent epithelial phenotype evident in AnkG cKO mouse lenses was the severely reduced and disrupted lateral membrane complexes between cells of the epithelial sheet (Fig. 5A). This abnormality results in the epithelium being filled with diffused proteins compared to the epithelium from littermate control lens which contains very symmetric columnar cells with well-developed lateral membrane assemblies and cell-cell junctions between adjacent cells (Fig. 5A). Having consistently observed this phenotype, we systematically evaluated the distribution and localization pattern of various proteins including membrane cytoskeletal linking protein (ezrin), cell adhesion (E-cadherin, N-cadherin, β-catenin, αE-catenin and ZO-1), gap junctional (connexin-50) and transport proteins (Na^+/K^+-ATPase) in the lens epithelium of AnkG cKO and littermate control specimens by immunofluorescence analysis. As shown in Fig. 5A, while each of the proteins listed above localized intensely either to the lateral membranes containing cell-cell junctions, apical or basal membranes in the control lens epithelium, these proteins were exhibited a very diffuse, cytosolic distribution in the AnkG cKO mouse lens epithelium, indicating that AnkG deficiency disrupts epithelial polarity, lateral membrane biogenesis and the organization of lateral membrane assemblies, spectrin cytoskeletal and transport proteins, ezrin and actin, in the lens epithelium. It is also evident from these images that deficiency of AnkG disrupts the basal, apical and basolateral distribution of most of the proteins described above in lens epithelium (Fig. 5A). AnkB, which also localizes to the cell-cell junctions and

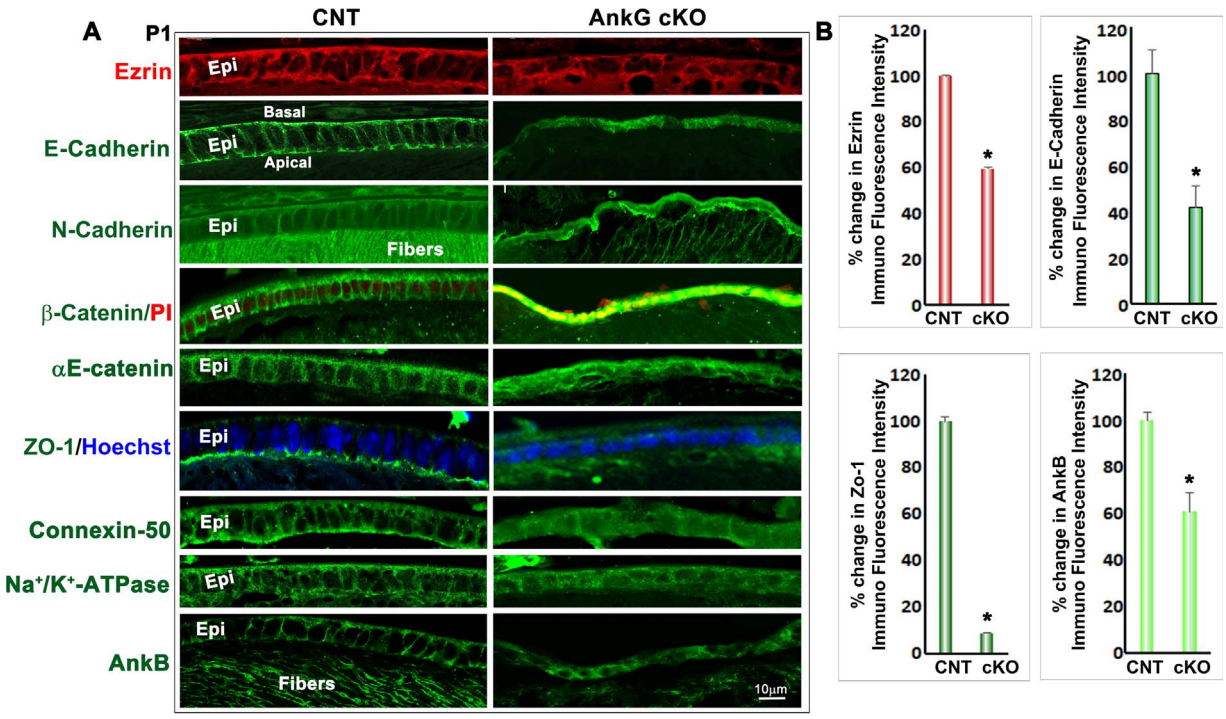

Fig. 5. AnkG cKO mouse lens epithelium reveals impaired lateral membrane assembly, cell-cell junctions and membrane targeting of transport and polarity proteins. A). To evaluate the impact of AnkG deficiency on lateral membrane assembly, cell-cell junctions and membrane organization of transport and polarity proteins within the lens epithelium, P1 lens specimens derived from AnkG cKO and control (CNT) mice were immunostained for proteins of interest as indicated in figure. While the staining pattern of different proteins described, localized discretely to the lateral membrane complexes, cell-cell junctions, basolateral and apical membranes in control lens epithelium, the staining was noted to be rather diffuse in AnkG deficient lens epithelium, with a lack of definitive lateral membrane complexes and cell-cell junctions, indicating extensive disruption of these cellular characteristics. B). Quantitative analysis of immunofluorescence of E-cadherin, AnkB, ezrin and Zo-1 in AnkG cKO mouse lens specimens showed a significant decrease compared to littermate control specimens (n = 5, *$p < 0.05$). Scale bars represent image magnification. PI: Propidium iodide.

basolateral membrane in control lens epithelium and shares many functional attributes with AnkG, failed to localize to the cell membrane in AnkG cKO mouse lens epithelium, exhibiting a diffuse distribution pattern (Fig. 5A). Unlike in the lens epithelium from P1 mouse lens that from P21 lenses exhibits cuboidal cells with decreased AnkB immunostaining that distributes to the basal region (Supplemental material; Fig. 3S). Additionally, the deficiency of AnkG appears to also have a direct or indirect impact on the levels of E-cadherin, ezrin, ankB and Zo-1 since the overall immunofluorescence staining intensity was reduced (by 58%, 40%, 39% and 90% respectively; based on immunofluorescence quantification) in the AnkG cKO lens epithelial specimens relative to control specimens (Fig. 5B). Both, the E15.5 and P1 lens specimens derived from AnkG cKO and littermate control mice were also stained with WGA and CellBrite stain, which revealed reduced lateral membrane height in AnkG deficient specimens starting from the embryonic stage and becoming very prominent in P1 specimens compared to respective controls (Supplemental material; Fig. 4S and 8S).

3.4. AnkG deficiency impairs lens epithelial cell proliferation, survival and plasticity

Based on the reduction in lens size and shortened epithelial sheet length of AnkG cKO lenses (Fig. 4), we speculated that AnkG deficiency very likely disrupts epithelial cell proliferation, survival and plasticity. To address this possibility, we evaluated apoptotic cell death by TUNEL labeling and quantitated and expressed results as percent change from control specimens per lens epithelium. Based on Hoechst staining (Fig. 6A and B), the total number of nuclei in P1 AnkG cKO mouse lens epithelium was also found to be significantly reduced (by ~ 25%; n = 6) compared to littermate control specimens. Consistent with this observation, as shown in Fig. 6C and D, while there were almost no detectable TUNEL positive cells (green fluorescence) in the control lens epithelium (P1), AnkG cKO lens specimens exhibited a robust and significant increase in TUNEL positive cells (bright yellow fluorescence in images merged with propidium iodide (red) staining; n = 5) throughout the entire epithelium of P1 specimens, confirming increased apoptotic epithelial cell death under AnkG deficiency. We also examined the E15.5 AnkG cKO lens specimens for TUNEL staining and found no TUNEL positive cells (see Supplemental figure; Fig. 4S).

To determine the status of epithelial cell proliferation in AnkG deficient mouse lenses, lens cryosections from P1 AnkG cKO and littermate control mice were immunostained using a specific monoclonal antibody directed against Ki-67, a well-characterized cell proliferation nuclear marker (Scholzen and Gerdes, 2000). As expected, control P1 lenses revealed a high level of immunopositive staining (green fluorescence) for Ki-67 at the germinative zone (equator) epithelium relative to the central epithelium, with the signal exhibiting a discrete nuclear localization (Fig. 6E and F). In contrast to the Ki-67 distribution observed in control specimens, it was noted that AnkG cKO lens specimens (P1) exhibited a much lower number of Ki-67 positive cells in the epithelium (~ 70% decrease; n = 8) compared to controls, indicating decreased epithelial cell proliferation associated with AnkG deficiency (Fig. 6E and F). Decreased lens epithelial proliferation under AnkG deficiency was found to be evident in the embryonic lenses (E15.5) as well (Supplemental material; Fig. 5S)

Given that the loss of E-cadherin and N-cadherin based cell-cell junctions in the AnkG cKO mouse lens epithelium (Fig. 5) could plausibly alter cell plasticity, fate and migration, we evaluated the expression of α-smooth muscle actin (αSMA), a well-recognized marker of myofibroblasts by immunostaining using a Cy-3 conjugated monoclonal antibody against α-SMA. As shown in Fig. 6G, α-SMA was undetectable in the control lenses, but readily detected throughout the epithelium (bright pinkish/red stain) in P1 AnkG cKO lens specimens, indicating altered cell plasticity and possible transdifferentiation of mouse lens epithelial cells into myofibroblasts under AnkG deficiency. The presumptive ciliary body (PCB) in Fig. 6G exhibits constitutive

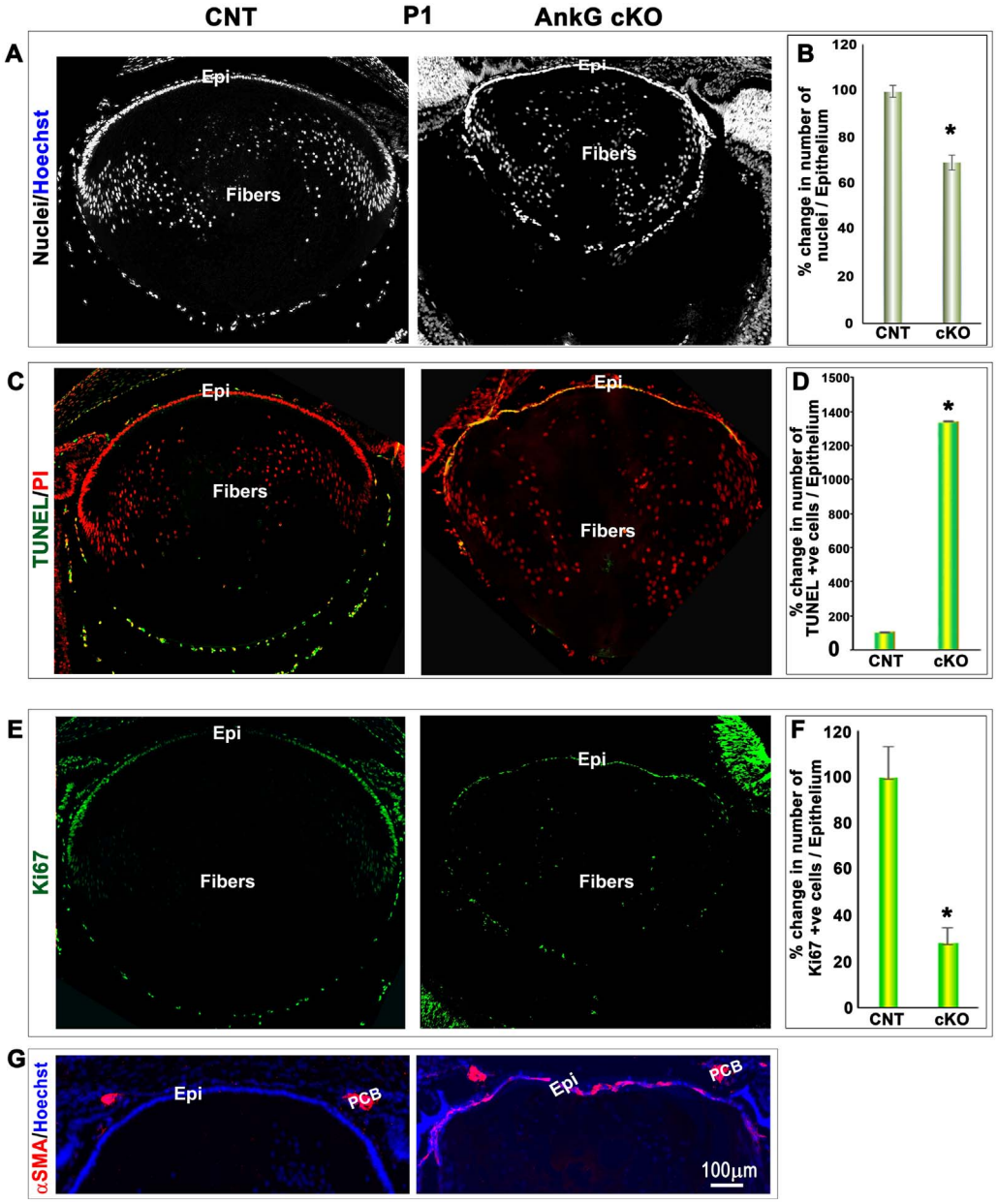

Fig. 6. AnkG deficiency impairs lens epithelial proliferation and survival and induces epithelial to mesenchymal transition. Having noted the reduction in lens size and an abnormal lens epithelial phenotype in AnkG cKO mice, evaluations were performed to determine the status of apoptotic cell death and proliferation within the lens epithelium by counting Hoechst stained nuclei, TUNEL positive cells and Ki-67 positive nuclei in P1 AnkG cKO mouse lenses and littermate control (CNT) specimens. A & B). Analysis of Hoechst stained nuclei in specimens from littermate control and AnkG cKO mice revealed a significant decrease (by ~ 30%, n = 6; *p < 0.05) in the number of total nuclei in the lens epithelium of AnkG deficient lenses compared to corresponding controls. C & D). Representative images of TUNEL staining from AnkG cKO and corresponding control mouse lenses, and quantitation of TUNEL positive cells in lens epithelium showed a significant increase in apoptotic cells under AnkG deficiency (n = 5; *P < 0.05). These specimens were also co-stained with propidium iodide (PI) to label cell nuclei. E & F). Quantitation of Ki-67 stained nuclei (green stain) using representative images of Ki-67 immunostained P1 lenses from AnkG cKO and corresponding control mice revealed a significant decrease (by ~ 70%; n = 8; * p < 0.05) in proliferating cells in the epithelium of AnkG deficient specimens compared to controls. G). Representative image of AnkG deficient P1 mouse lens showing immunopositive staining for α-SMA (bright pink) in the epithelium relative to a control specimen, in which staining for α-SMA is absent. In both specimens, the presumptive ciliary body (PCB) which is known to express αSMA constitutively, immunostains positively for the protein. These specimens were also co-stained with Hoechst (blue stain). Scale bar indicates image magnification.

expression of αSMA in both AnkG cKO and control mouse specimens. Additionally, while αSMA expression and distribution was detectable in the E15.5 AnkG cKO lens epithelium it was significantly lower compared to that in P1 specimens AnkG cKO lens epithelium, and absent from control specimens (Fig. 5S). Moreover, we also co-labeled lens specimens (both E15.5 and P1) with Ki67 and αSMA and found both Ki67 positive and negative cells showed positive staining for αSMA, indicating αSMA expression is induced in both proliferating and non-proliferating AnkG deficient cells, perhaps at different stages of plasticity (Fig. 5S).

3.5. AnkG deficiency disrupts organization but not differentiation of lens fiber cells

Differentiation is a major event in lens development, during which epithelial cells at the germinative zone exit from the cell cycle and start differentiating into elongated secondary fibers and expressing various fiber-specific proteins including crystallins, aquaporin-0 and beaded filament proteins (filensin and phakanin). Subsequently, these elongating fibers undergo maturation and terminal differentiation, with the bulk of the lens being comprised of fiber cells (Cvekl and Ashery-Padan,

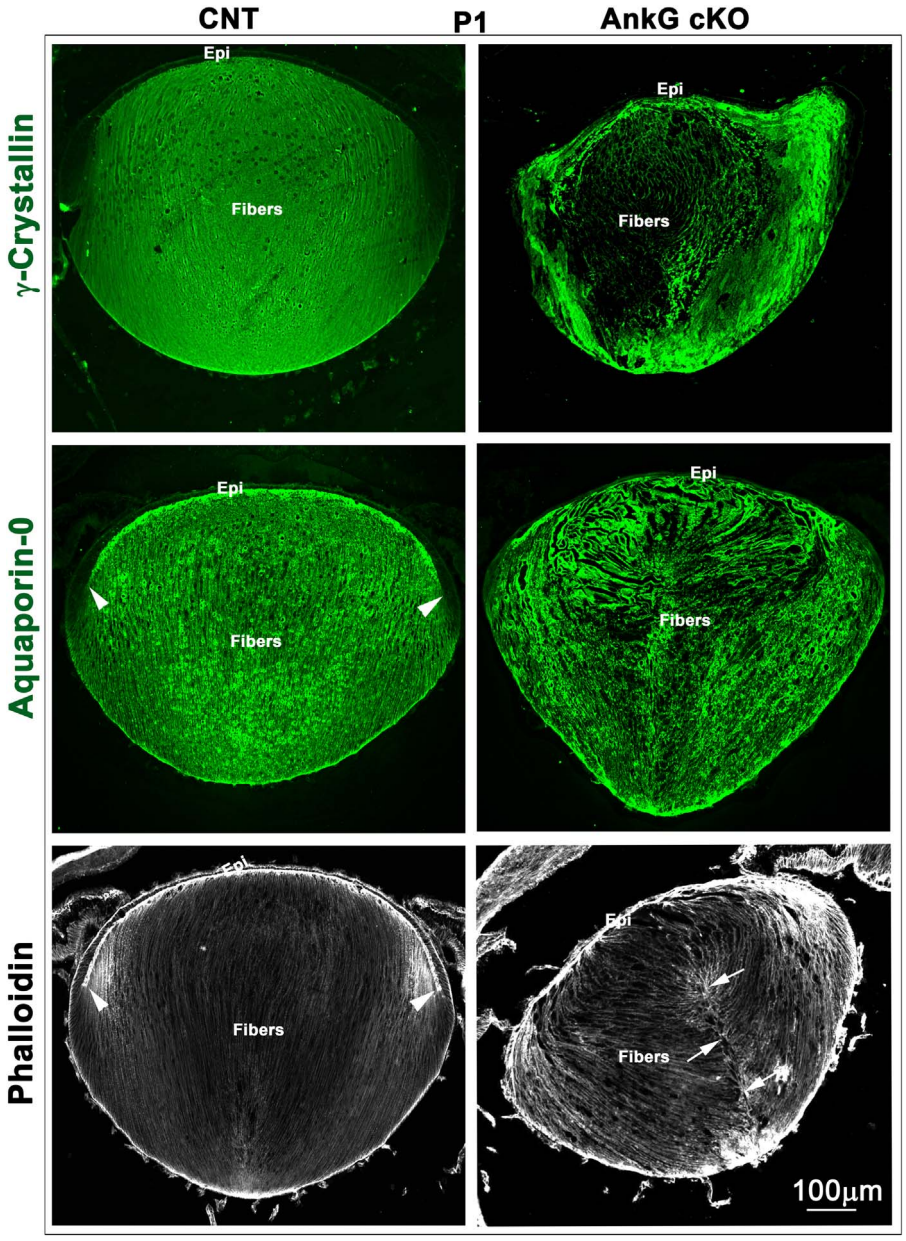

Fig. 7. AnkG deficiency disrupts mouse lens fulcrum formation, fiber cell organization and suture formation with no overt changes in differentiation. To determine the possible influence of AnkG in lens differentiation, P1 AnkG cKO and littermate control (CNT) mouse lens specimens were immunostained for fiber cell differentiation specific markers (aquaporin-0 and γ-crystallin). Both these specimens exhibited a robust staining for the differentiation markers (representative images are shown) indicating that AnkG deficiency is not associated with major changes in lens differentiation. AnkG deficient lenses (from P1 mouse) however, revealed disorganized lens fibers with sutural defects (indicated with arrows) when compared to corresponding control specimens, as shown in the bottom image derived from tissue sections stained with rhodamine-phalloidin. Similarly, fulcrum formation is disrupted in lenses under AnkG deficiency relative to what is noted in control lenses (indicated with arrow heads). Scale bar represents image magnification.

2014). To assess whether AnkG deficiency impacts lens fiber cell differentiation, we evaluated the expression and distribution of lens differentiation-specific markers γ-crystallin and aquaporin-0 in P1 AnkG cKO mouse lenses using appropriate antibodies. As shown in Fig. 7, similar to littermate control lenses, AnkG cKO mouse lenses also revealed robust expression of both γ-crystallin and aquaporin-0, indicating that a largely normal lens differentiation process takes place under AnkG deficiency.

Although lens fiber cell differentiation appears to not exhibit any overt deficits in AnkG cKO mouse lenses, the migration and organization pattern of fiber cells was found to be abnormal in these lenses. Figs. 4A and 7 (specimens stained for F-actin with rhodamine-phalloidin) show fiber cell organization in AnkG deficient lenses relative to control lenses. It is evident from the images shown in Figs. 3, 4 and 7 and in Fig. 7S that lens fulcrum (the area where the apical tips of early elongating secondary fibers fuse with epithelium at the lens equator; (Sugiyama et al., 2009)) and secondary fiber cell migration and organization patterns are abnormal and appear to affect suture formation in AnkG deficient lenses, relative to that observed in the control lenses (Fig. 7; indicated with arrows in bottom panel and arrow heads indicate lens fulcrum). It is possible that the defective cell adhesive interactions between the apical regions of the epithelial cells and fiber cells along with the noted defective fulcrum, actin cytoskeletal organization and ZO-1 distribution, are partly responsible for the observed changes in lens fiber cell orientation and migration under AnkG deficiency.

4. Discussion and conclusion

The main objective of this study was to explore the role of AnkG in epithelial organogenesis and architecture using the ocular lens as a model

system. Given that AnkG plays a vital role in epithelial cell-cell adhesive interactions, E-cadherin membrane localization and endocytosis, and lateral membrane biogenesis (Cadwell et al., 2016; Jenkins et al., 2015; Kizhatil and Bennett, 2004; Kizhatil et al., 2007a), we hypothesized that AnkG might have an obligatory role in lens morphogenesis and growth. To investigate this possibility, we targeted AnkG expression in a lens-specific manner using the LoxP-Cre approach to evaluate the direct impact of AnkG deficiency on lens morphogenesis, growth and integrity in a mouse model. Lenses deficient in AnkG, which distributes predominantly to the lens epithelium and exhibits intense localization to the lateral membranes, revealed dramatic defects including shortened epithelial height, sheet length, loss of adherens junctions, disrupted lateral membrane complexes, and impaired membrane organization of transport and adhesion proteins, together with increased apoptotic cell death and epithelial transdifferentiation leading to impaired lens morphogenesis, shape and growth. To the best of our knowledge, this is the first study illuminating an essential role for AnkG-regulated lateral membrane assembly, spectrin, cell adhesion, polarity and transport protein membrane organization in controlling and maintaining lens development, growth, shape and integrity.

The findings from this study, together with our previous work on AnkB deficient lenses (Maddala et al., 2016), provide evidence that both AnkG and AnkB play distinct and crucial roles in lens development, growth and integrity. The distinct effects of AnkG and AnkB in development, growth and integrity of the ocular lens appear to be directly related to their differential distribution within the lens. While AnkG exhibits a predominant distribution to the epithelium, AnkB distributes more abundantly to mouse lens fibers cells relative to the epithelium (Maddala et al., 2016; More et al., 2001). Moreover, unlike the overt phenotype that we observed under AnkG deficiency in embryonic and neonatal mouse lenses, AnkB cKO mouse lenses do not exhibit a noticeable phenotype earlier than the P12 stage (unpublished data, manuscript in preparation). These observations indicate that although AnkG and AnkB share many functional domains (Bennett and Lorenzo, 2016), AnkB does not compensate for AnkG deficiency in the maintenance of lens epithelial phenotype. Since all of the prominent AnkG isoforms detected in our study (ranging from ~ 300 to 50 kDa) were found to be dramatically reduced in AnkG cKO mouse lenses compared to wild type lenses, it is not clear whether the lens phenotype noted in the AnkG cKO mice is due to an overall deficiency across all or specific isoforms of AnkG.

It is noteworthy that the Cre transgenic mice used in this study were shown to express Cre recombinase starting from embryonic day 8.75, including in the surface ectoderm and lens pit and vesicle (Ashery-Padan et al., 2000). We confirmed AnkG protein expression in the lens vesicle with distribution localizing intensely to the presumptive epithelial apical lateral membrane complexes (indicated with arrows in Fig. 1G and Fig. 1S). Although we consistently recorded AnkG distribution to the apical regions of lens epithelium, the significance of this distribution pattern for lens morphogenesis is uncertain. Additionally, the noticeable phenotype in AnkG cKO mice appears only from the E15.5 stage indicating that AnkG might not impact early lens development and lens vesicle separation from the overlying surface ectoderm, but likely plays a critical role in late embryonic lens morphogenesis, especially in maintenance of lens growth and shape by regulating establishment of the epithelial phenotype. However, proteins involved in maintaining epithelial apical polarity have been demonstrated to impact not only morphogenesis but also secretion, directional transport and ciliogenesis (Yano et al., 2017). Thus, further studies are needed to determine which AnkG isoform(s) distribute to the apical region of the lens epithelium and identify AnkG binding proteins.

Interestingly, the phenotype of the AnkG cKO mouse lens was found to be very similar to that of E-cadherin cKO mouse lenses which were developed using the same Cre transgenic mice used in this study (Pontoriero et al., 2009). Both AnkG and E-cadherin cKO mice exhibit microphthalmic eyes with decreased lens weight. Similarly, like the AnkG cKO mice, E-cadherin cKO mice have also been reported to exhibit no noticeable lens abnormality prior to the E15.5 stage (Pontoriero et al., 2009). However, postnatal lenses from both AnkG deficient (Fig. 3) and E-cadherin cKO mouse models (Pontoriero et al., 2009) reveal severe defects in lens integrity with accumulation of large vacuoles in the fiber cells. Moreover, similar to lenses from AnkG cKO mice, E-cadherin cKO mouse lenses have been shown to exhibit impaired cell-cell junctions, disrupted ZO-1 and β-catenin distribution in the lens epithelium, together with transdifferentiation and expression of α-SMA in the lens epithelium (Pontoriero et al., 2009). Collectively these data reveal that AnkG deficiency mimics the E-cadherin deficiency-induced phenotype and cellular changes in the lens epithelium, further supporting the importance of cell-cell junctions, polarity and lateral membrane assembly in the regulation of lens morphogenesis by AnkG and E-cadherin.

Although our ability to utilize biochemical analyses to demonstrate how the absence of AnkG impairs lens phenotypes was hampered due to the observed phenotype in neonatal lenses, the histological and immunofluorescence based analyses convincingly supported the importance of AnkG-regulated epithelial cell lateral membrane assembly, biogenesis, E-cadherin-based cell-cell junctions, membrane organization of the actin-spectrin cytoskeleton, polarity protein (Zo-1), transport and other adhesion proteins in establishment of the lens epithelial phenotype. Studies using MDCK (Madin-Darby Canine Kidney) cells have elegantly and mechanistically demonstrated that AnkG together with β-spectrin and the palmitoylation and phosphoinositide lipid binding characteristics, respectively, of these proteins, regulate lateral membrane biogenesis and assembly, and inhibit endocytosis, and that both proteins interact directly with E-cadherin (Cadwell et al., 2016; He et al., 2014; Jenkins et al., 2015; Kizhatil and Bennett, 2004; Kizhatil et al., 2007a). Based on these prior studies, we assume that absence of AnkG in the lens epithelium impacts epithelial phenotype via similar mechanisms as has been demonstrated in MDCK cells. The results of CellBrite and WGA labeling of AnkG cKO mouse lens epithelial specimens in fact, reveal compromised lateral membrane height and decreased staining of WGA in AnkG deficient lenses relative to control lenses, supporting the importance of AnkG in regulation of lateral membrane assembly and biogenesis. Disruption of actin and β-spectrin localization to the lens epithelial lateral membrane was evident in the AnkG cKO mouse lens epithelium supporting the well-established function of ankyrins in targeting the actin-spectrin cytoskeleton to the membrane proteins (Bennett and Baines, 2001). Although we did not directly explore the involvement of phosphoinositide lipids in lens epithelial lateral membrane assembly and biogenesis, disrupted organization of spectrin may partly account for the impaired lateral membrane assembly and reduced epithelial height of the AnkG cKO lens epithelium since phosphoinositide lipids are required for lateral membrane organization and assembly (Bennett and Lorenzo, 2016), and spectrin is recognized to bind phosphoinositides via its pleckstrin homology (PH) domain. Taken together, the results of this study demonstrate a crucial role for AnkG in epithelial organogenesis, growth, survival and architecture. Earlier studies have shown the importance of interactions of AnkG with connexins (Sato et al., 2011) and Na/K-ATPase (Devarajan et al., 1994; Stabach et al., 2008), and the role of these interactions in membrane targeting of connexins and Na/K-ATPase. Consistent with these earlier studies, our findings demonstrate that in the absence of AnkG, connexin-50, Na^+/K^+-ATPase, ZO-1, catenins and ezrin failed to localize to the basolateral and apical membranes in AnkG cKO mouse lenses, leading to abnormalities of lens morphogenesis and cytoarchitecture.

The increased apoptosis in conjunction with decreased proliferation recorded in AnkG cKO lens epithelial cells could owe partly to impaired cell-cell junctions and polarity observed under AnkG deficiency. The shortened epithelial sheet length observed in AnkG cKO mice appears to impact lens shape, resulting in the conversion from a spherical to conical phenotype (Fig. 7). Similarly, the disorganization of lens fibers noted in

AnkG cKO lenses is likely a direct result of disrupted epithelial and fiber cell apical to apical adhesive interactions under AnkG deficiency as well as impaired formation of the lens fulcrum in these mice. This conclusion is supported in part by the noted changes in membrane organization of ZO-1 and actin at the interface of epithelium and fibers in AnkG cKO mouse lenses (Figs. 5 and 7). Additionally, the accumulation of large vacuoles in the lens cortical and nuclear area in postnatal (P10 and P21; Fig. 3) AnkG cKO lenses appears to result from the defects noted in lens fiber cell organization and sutures in these mice (Fig. 7). Interestingly, the lens epithelial defects resulting from the absence of AnkG appear to not impact lens fiber cell differentiation in any significant manner based on the normal expression and distribution pattern of aquaporin-0 and γ-crystallin, known markers of fiber cell differentiation (Cvekl and Ashery-Padan, 2014), in AnkG cKO lens fiber cells.

In conclusion, this study provides genetic evidence for a vital and distinct role for AnkG in lens morphogenesis, growth and integrity via regulating establishment of the lens epithelial phenotype.

Acknowledgments

We thank Jianming Qiu for her help in maintaining the AnkG cKO mouse colony, and performing genotyping analysis and tissue sectioning, and Samuel Zigler, Ph.D., Harold Erickson and Joe Horwitz, Ph.D. for providing γ-crystallin, Laminin and aquaporin-0 antibodies, respectively. We also greatly appreciate Ruth Ashery-Padan, Ph.D., for her generous permission to use the Le-Cre transgenic mice in this study.

Funding

This work was funded by the National Institutes of Health (R01EY025096, R21EY027053 and P30-EY005722).

Declaration of interest

None.

Appendix A. Supporting information

Supplementary data associated with this article can be found in the online version at doi:10.1016/j.ydbio.2018.12.016.

References

Ashery-Padan, R., Marquardt, T., Zhou, X., Gruss, P., 2000. Pax6 activity in the lens primordium is required for lens formation and for correct placement of a single retina in the eye. Genes Dev. 14, 2701–2711.
Bassnett, S., Shi, Y., Vrensen, G.F., 2011. Biological glass: structural determinants of eye lens transparency. Philos. Trans. R. Soc. Lond. Ser. B Biol. Sci. 366, 1250–1264.
Bennett, V., Baines, A.J., 2001. Spectrin and ankyrin-based pathways: metazoan inventions for integrating cells into tissues. Physiol. Rev. 81, 1353–1392.
Bennett, V., Healy, J., 2009. Membrane domains based on ankyrin and spectrin associated with cell-cell interactions. Cold Spring Harb. Perspect. Biol. 1, a003012.
Bennett, V., Lorenzo, D.N., 2016. An adaptable spectrin/ankyrin-based mechanism for long-range organization of plasma membranes in vertebrate tissues. Curr. Top. Membr. 77, 143–184.
Braga, V., 2000. Epithelial cell shape: cadherins and small GTPases. Exp. Cell Res. 261, 83–90.
Cadwell, C.M., Jenkins, P.M., Bennett, V., Kowalczyk, A.P., 2016. Ankyrin-G inhibits endocytosis of cadherin dimers. J. Biol. Chem. 291, 691–704.
Chauhan, B., Plageman, T., Lou, M., Lang, R., 2015. Epithelial morphogenesis: the mouse eye as a model system. Curr. Top. Dev. Biol. 111, 375–399.
Cheng, C., Nowak, R.B., Fowler, V.M., 2017. The lens actin filament cytoskeleton: diverse structures for complex functions. Exp. Eye Res. 156, 58–71.
Cunha, S.R., Mohler, P.J., 2009. Ankyrin protein networks in membrane formation and stabilization. J. Cell. Mol. Med. 13, 4364–4376.
Cvekl, A., Ashery-Padan, R., 2014. The cellular and molecular mechanisms of vertebrate lens development. Development 141, 4432–4447.
Cvekl, A., Zhang, X., 2017. Signaling and gene regulatory networks in mammalian lens development. Trends Gen. TIG 33, 677–702.
Devarajan, P., Scaramuzzino, D.A., Morrow, J.S., 1994. Ankyrin binds to two distinct cytoplasmic domains of Na,K-ATPase alpha subunit. Proc. Natl. Acad. Sci. USA 91, 2965–2969.
He, M., Abdi, K.M., Bennett, V., 2014. Ankyrin-G palmitoylation and betaII-spectrin binding to phosphoinositide lipids drive lateral membrane assembly. J. Cell Biol. 206, 273–288.
Jenkins, P.M., He, M., Bennett, V., 2015. Dynamic spectrin/ankyrin-G microdomains promote lateral membrane assembly by opposing endocytosis. Sci. Adv. 1, e1500301.
Jenkins, P.M., Vasavda, C., Hostettler, J., Davis, J.Q., Abdi, K., Bennett, V., 2013. E-cadherin polarity is determined by a multifunction motif mediating lateral membrane retention through ankyrin-G and apical-lateral transcytosis through clathrin. J. Biol. Chem. 288, 14018–14031.
Kizhatil, K., Bennett, V., 2004. Lateral membrane biogenesis in human bronchial epithelial cells requires 190-kDa ankyrin-G. J. Biol. Chem. 279, 16706–16714.
Kizhatil, K., Davis, J.Q., Davis, L., Hoffman, J., Hogan, B.L., Bennett, V., 2007a. Ankyrin-G is a molecular partner of E-cadherin in epithelial cells and early embryos. J. Biol. Chem. 282, 26552–26561.
Kizhatil, K., Yoon, W., Mohler, P.J., Davis, L.H., Hoffman, J.A., Bennett, V., 2007b. Ankyrin-G and beta2-spectrin collaborate in biogenesis of lateral membrane of human bronchial epithelial cells. J. Biol. Chem. 282, 2029–2037.
Knust, E., 2000. Control of epithelial cell shape and polarity. Curr. Opin. Genet. Dev. 10, 471–475.
Kordeli, E., Lambert, S., Bennett, V., 1995. AnkyrinG. A new ankyrin gene with neural-specific isoforms localized at the axonal initial segment and node of Ranvier. J. Biol. Chem. 270, 2352–2359.
Logan, C.M., Rajakaruna, S., Bowen, C., Radice, G.L., Robinson, M.L., Menko, A.S., 2017. N-cadherin regulates signaling mechanisms required for lens fiber cell elongation and lens morphogenesis. Dev. Biol. 428, 118–134.
Lovicu, F.J., McAvoy, J.W., de Iongh, R.U., 2011. Understanding the role of growth factors in embryonic development: insights from the lens. Philos. Trans. R. Soc. Lond. Ser. B Biol. Sci. 366, 1204–1218.
Maddala, R., Chauhan, B.K., Walker, C., Zheng, Y., Robinson, M.L., Lang, R.A., Rao, P.V., 2011. Rac1 GTPase-deficient mouse lens exhibits defects in shape, suture formation, fiber cell migration and survival. Dev. Biol. 360, 30–43.
Maddala, R., Nagendran, T., Lang, R.A., Morozov, A., Rao, P.V., 2015. Rap1 GTPase is required for mouse lens epithelial maintenance and morphogenesis. Dev. Biol. 406, 74–91.
Maddala, R., Rao, P.V., 2017. Switching of alpha-catenin from epithelial to neuronal type during lens epithelial cell differentiation. Invest. Ophthalmol. Vis. Sci. 58, 3445–3455.
Maddala, R., Walters, M., Brophy, P.J., Bennett, V., Rao, P.V., 2016. Ankyrin-B directs membrane tethering of periaxin and is required for maintenance of lens fiber cell hexagonal shape and mechanics. American journal of physiology. Cell Physiol. 310, C115–C126.
More, M.I., Kirsch, F.P., Rathjen, F.G., 2001. Targeted ablation of NrCAM or ankyrin-B results in disorganized lens fibers leading to cataract formation. J. Cell Biol. 154, 187–196.
Nelson, W.J., Dickinson, D.J., Weis, W.I., 2013. Roles of cadherins and catenins in cell-cell adhesion and epithelial cell polarity. Prog. Mol. Biol. Transl. Sci. 116, 3–23.
Pispa, J., Thesleff, I., 2003. Mechanisms of ectodermal organogenesis. Dev. Biol. 262, 195–205.
Pontoriero, G.F., Smith, A.N., Miller, L.A., Radice, G.L., West-Mays, J.A., Lang, R.A., 2009. Co-operative roles for E-cadherin and N-cadherin during lens vesicle separation and lens epithelial cell survival. Dev. Biol. 326, 403–417.
Rao, P.V., Maddala, R., 2006. The role of the lens actin cytoskeleton in fiber cell elongation and differentiation. Semin. Cell Dev. Biol. 17, 698–711.
Rodriguez-Boulan, E., Nelson, W.J., 1989. Morphogenesis of the polarized epithelial cell phenotype. Science 245, 718–725.
Sato, P.Y., Coombs, W., Lin, X., Nekrasova, O., Green, K.J., Isom, L.L., Taffet, S.M., Delmar, M., 2011. Interactions between ankyrin-G, Plakophilin-2, and Connexin43 at the cardiac intercalated disc. Circ. Res. 109, 193–201.
Scholzen, T., Gerdes, J., 2000. The Ki-67 protein: from the known and the unknown. J. Cell. Physiol. 182, 311–322.
Stabach, P.R., Devarajan, P., Stankewich, M.C., Bannykh, S., Morrow, J.S., 2008. Ankyrin facilitates intracellular trafficking of alpha1-Na+-K+-ATPase in polarized cells. Am. J. Physiol. Cell Physiol. 295, C1202–C1214.
Sugiyama, Y., Akimoto, K., Robinson, M.L., Ohno, S., Quinlan, R.A., 2009. A cell polarity protein aPKClambda is required for eye lens formation and growth. Dev. Biol. 336, 246–256.
Sugiyama, Y., Lovicu, F.J., McAvoy, J.W., 2011. Planar cell polarity in the mammalian eye lens. Organogenesis 7, 191–201.
Sugiyama, Y., Prescott, A.R., Tholozan, F.M., Ohno, S., Quinlan, R.A., 2008. Expression and localisation of apical junctional complex proteins in lens epithelial cells. Exp. Eye Res. 87, 64–70.
Tseng, W.C., Jenkins, P.M., Tanaka, M., Mooney, R., Bennett, V., 2015. Giant ankyrin-G stabilizes somatodendritic GABAergic synapses through opposing endocytosis of GABAA receptors. Proc. Natl. Acad. Sci. USA 112, 1214–1219.
White, T.W., Gao, Y., Li, L., Sellitto, C., Srinivas, M., 2007. Optimal lens epithelial cell proliferation is dependent on the connexin isoform providing gap junctional coupling. Invest. Ophthalmol. Vis. Sci. 48, 5630–5637.
Yano, T., Kanoh, H., Tamura, A., Tsukita, S., 2017. Apical cytoskeletons and junctional complexes as a combined system in epithelial cell sheets. Ann. N Y Acad. Sci. 1405, 32–43.
Zhang, Y., Fan, J., Ho, J.W., Hu, T., Kneeland, S.C., Fan, X., Xi, Q., Sellarole, M.A., de Vries, W.N., Lu, W., Lachke, S.A., Lang, R.A., John, S.W., Maas, R.L., 2016. Crim1 regulates integrin signaling in murine lens development. Development 143, 356–366.